Numerical Examination of Cross-Ply Sisal Fibre/Epoxy Composite Laminates with Cohesive Zone Elements at Low-Velocity Impact Loading

Enock A. Duodu

Department of Mechanical and Automotive Engineering, Akenten Appiah-Menka University of Skills Training and Entrepreneurial Development, Ghana

Abstract:

The paper focuses on modelling damage evolution in composite laminates under low-velocity impact, specifically cross-ply configurations. A finite element model is developed to simulate interlaminar delamination and assess the damage mechanisms under varying impact energy levels. The cohesive zone model (CZM) is used to accurately capture delamination initiation and progression. It discusses the implementation of damage models for intra- and inter-laminar mechanisms and the use of cohesive zone elements to simulate matrix cracking and splitting. The results highlight the influence of fibre orientation, laminate stacking sequence, and cohesive parameters on the energy absorption and damage propagation. This paper provides valuable insights into the impact performance of bio-composites, aiding their implementation in lightweight and sustainable structural applications.

Keywords: Cohesive elements, finite element analysis, inter-laminar, intra-laminar, natural fibre

1. Introduction

The growing environmental concerns and the need for sustainable engineering solutions have led to significant interest in natural fibre-reinforced polymer (NFRP) composites. Among the various natural fibres, sisal has gained attention due to its high tensile strength, availability, and biodegradability. Sisal fibres, when combined with polymer matrices such as epoxy, exhibit promising mechanical properties, making them suitable for lightweight and environmentally friendly applications in automotive, aerospace, and construction industries[1-3]. Composite laminates subjected to low-velocity impacts often experience significant damage, including delamination, matrix cracking, and fibre breakage. Such damage mechanisms can degrade structural integrity and reliability. Therefore, understanding the impact behavior of NFRP laminates is crucial. Numerical methods, particularly finite element analysis (FEA), have emerged as powerful tools for studying impact responses in composite materials. Recent advancements in cohesive zone models (CZM) have enhanced the ability to simulate delamination accurately [4]. In NFRP composites, the incorporation of natural fibres into such configurations has shown potential for structural applications, particularly in automotive, aerospace, and civil engineering sectors.

However, one of the critical challenges in composite laminate structures is their susceptibility to interlaminar damage, such as delamination, when subjected to out-of-plane loading. Low-velocity impact events, such as tool drops or debris impacts, can cause significant internal damage that is often not visible on the surface but can severely degrade the structural integrity of the material. Understanding and predicting the damage mechanisms in NFRP laminates under such loading conditions are essential for ensuring their safe and reliable application.

Numerical methods, particularly finite element analysis (FEA), have emerged as powerful tools for investigating the mechanical behavior of composite materials. These methods enable researchers to simulate complex loading scenarios, predict damage initiation and propagation, and optimize material designs. Among the various numerical approaches, cohesive zone modeling (CZM) has proven effective in simulating interlaminar delamination, a critical failure mode in composite laminates [5]. CZM employs cohesive elements with predefined traction-separation laws to model the initiation and progression of delamination under various loading conditions.

Several studies have demonstrated the application of CZM in synthetic fibre-reinforced composites, such as carbon/epoxy[6-9] and glass/epoxy [10-14] systems, to predict delamination under impact loading. However, there is limited research on its application to NFRP composites, particularly sisal fibre/epoxy laminates. Furthermore, while experimental studies on the impact behavior of natural fibre composites are relatively

common, numerical studies incorporating advanced damage modeling techniques remain sparse. This gap highlights the need for a detailed investigation into the use of cohesive elements for simulating delamination in sisal/epoxy laminates under low-velocity impact.

Despite the growing interest in NFRP composites, significant gaps exist in the literature regarding their impact behaviour and damage mechanisms under low-velocity impact. Most studies have focused on experimental investigations [14-19], which, while valuable, but often limited by their inability to provide detailed insights into internal damage mechanisms. Numerical methods, particularly those incorporating CZM, offer a complementary approach that can overcome these limitations. However, the application of CZM to predict delamination in crossply sisal/epoxy laminates has not been adequately explored.

In view of the limited studies, this paper developed a finite element model based on continuum damage mechanics (CDM) to simulate the low velocity impact damage in cross-ply sisal composite laminates. Damage-friction interface constitutive model is integrated into the model to involve apparent friction generated at the debonding interfaces under compressive impact loading. The intra-laminar and inter-laminar damage models are coded in a user-material subroutine VUMAT on ABAQUS/Explicit platform to predict damage initiation and evolution. The numerical predictions are in acceptable agreement with the experimental data in terms of impact energy-time, force-time and force-displacement curves, which verifies the efficiency of the proposed finite element model. Since the present numerical analysis model is generic in nature, it can be extended to study the low velocity impact behaviour in other types of composite laminates.

2. Damage Models and Formulations

Low velocity impact can be defined as a quasi-static response and characterized by dynamic events with large mass and low velocity. In low-velocity impact, the contact duration takes relatively long period for the entire structure to respond to impact and consequently absorbs more energy. The damage modes of composite laminates under low velocity impact can generally be grouped into intra-laminar damage (matrix cracking and fibre breaking) and inter-laminar damage (delamination). The impact damage process can be simulated by damage models, which consists of damage initiation criterion and damage evolution law.

2.1 Intra-ply damage

The widely used 3D Hashin failure criteria in Ref. [20] was adopted and modified by incorporating the strain rate-dependent strength and stiffness properties to trigger the damage initiation modes, and defined as follow:

Fibre tensile failure ($\sigma_{11} \ge 0$)

$$F_{fi} = \left(\frac{\sigma_1}{X_T}\right)^2 + \alpha \left(\frac{\sigma_{12}}{S_{12}}\right)^2 + \alpha \left(\frac{\sigma_{13}}{S_{13}}\right)^2 \ge 1 \tag{1}$$

Fibre compressive failure ($\sigma_{11} < 0$)

$$F_{fc} = \left(\frac{\sigma_1}{X_C}\right)^2 \ge 1 \tag{2}$$

Matrix tensile failure $(\sigma_{22} + \sigma_{33} \ge 0)$

$$F_{mt} = \left(\frac{\sigma_2 + \sigma_3}{Y_T}\right)^2 + \left(\frac{1}{S_{23}^2}\right) \left(\sigma_{23}^2 - \sigma_{22}\sigma_{33}\right) + \left(\frac{\sigma_{12}}{S_{12}}\right)^2 + \left(\frac{\sigma_{13}}{S_{13}}\right)^2 \ge 1 \tag{3}$$

Matrix compressive failure ($\sigma_{22} + \sigma_{33} < 0$

$$F_{mc} = \left(\frac{\sigma_2 + \sigma_3}{2S_{23}}\right)^2 + \left(\frac{\sigma_2 + \sigma_3}{Y_C}\right) \left[\left(\frac{Y_C}{2S_{23}}\right)^2 - 1\right] + \frac{1}{S_{23}^2} \left(\sigma_{23}^2 - \sigma_2\sigma_3\right) + \left(\frac{\sigma_{12}}{S_{12}}\right)^2 + \left(\frac{\sigma_{13}}{S_{13}}\right)^2 \ge 1$$
(4)

In Equations (1-4), X_T and X_C are the tensile and compressive strengths in fibre direction; Y_T and Y_C are the tensile and compressive strengths in transverse direction; S_{12} , S_{13} and S_{23} are the shear strengths respectively; α is the shear failure coefficient applied to determine the contribution of shear stresses on the fibre tensile failure.

Once the damage initiation criterion is reached, the damage development requires a damage evolution law. Herein, a gradual degradation scheme coupling with Murakami damage model [21] proposed by Lapczyk et al. [22] and Fang et al. [23] is applied to characterize the intra-laminar damage evolution. The damage variable for each failure mode is expressed as:

$$d_{I} = \frac{\delta_{I,eq}^{f}(\delta_{I,eq} - \delta_{I,eq}^{0})}{\delta_{I,eq}(\delta_{I,eq}^{f} - \delta_{I,eq}^{0})} \qquad (d_{I} \in [0,1], \qquad I = ft, fc, mt, mc)$$
 (5)

where $\delta_{\mathrm{I},eq}^0$ is the equivalent displacement for damage initiation; $\delta_{\mathrm{I},eq}^f$ is the equivalent displacement at final failure; and they can be determined by

$$\delta_{\text{L},eq}^0 = \delta_{\text{L},eq} / \sqrt{F_{\text{I}}} \tag{6}$$

$$\delta_{\mathrm{I},eq}^{f} = 2G_{\mathrm{I}} / (\sigma_{\mathrm{I},eq} / \sqrt{F_{\mathrm{I}}}) \tag{7}$$

where $F_{\rm I}$ is the value of damage initiation criterion; $G_{\rm I}$ is the fracture energy density; $\delta_{{\rm I},eq}$ and $\sigma_{{\rm I},eq}$ are the equivalent displacement and equivalent stress for a failure mode respectively, and expressions are given in Ref. [23].

2.2 Inter-ply damage

The cohesive zone elements are adopted to simulate the inter-laminar delamination behaviour at the interface of adjacent layers in the composite laminates. The traction stress and separation displacement of the nodes on the interface are governed by traction-separation model consisting of damage initiation criterion and damage evolution law. Actually, delamination propagation is likely to take place under mixed-mode loading thus delamination initiation and the corresponding reduction behaviour are determined by damage modes I, II and III simultaneously. For the mixed-mode loading, the current effective relative displacement, δ_m , is introduced as

$$\delta_{\rm m} = \sqrt{\left\langle \delta_1 \right\rangle^2 + \delta_2^2 + \delta_3^2} \tag{8}$$

where the symbol <> represents the Macaulay operator.

For a linear reduction process, the damage variable d for damage evolution is expressed by

$$d = \frac{\delta_{\mathrm{m}}^{\mathrm{f}}(\delta_{\mathrm{m}}^{\mathrm{max}} - \delta_{\mathrm{m}}^{0})}{\delta_{\mathrm{m}}^{\mathrm{max}}(\delta_{\mathrm{m}}^{\mathrm{f}} - \delta_{\mathrm{m}}^{0})} \qquad (d \in [0, 1])$$
(9)

where δ_{m}^{0} and δ_{m}^{f} are the effective relative displacements of interface at damage initiation and complete failure; and the maximum current relative displacement δ_{m}^{max} is defined as $\delta_{m}^{max} = max \left\{ \delta_{m}^{max}, \, \delta_{m} \right\}$ regarding the damage irreversibility.

A quadratic stress criterion is used to determine the damage initiation displacement, i.e. δ_m^0 , of the interface, which is given by

$$\left(\frac{\left\langle t_1 \right\rangle}{N}\right)^2 + \left(\frac{t_2}{S}\right)^2 + \left(\frac{t_3}{T}\right)^2 = 1 \tag{10}$$

here t_1 , t_2 and t_3 represent the normal and shear stresses, respectively. N, S and T denote the interface tensile and shear strengths.

An interactive power law of energy is applied to determine the final displacement, i.e. δ_m^f , of the interface, which is given by

$$\left(\frac{G_{\rm I}}{G_{\rm IC}}\right)^2 + \left(\frac{G_{\rm II}}{G_{\rm IIC}}\right)^2 + \left(\frac{G_{\rm III}}{G_{\rm IIIC}}\right)^2 = 1$$
(11)

where $G_{\rm I}$, $G_{\rm II}$ and $G_{\rm III}$ are the current energy release rates of mode I, II and III while $G_{\rm IC}$, $G_{\rm IIC}$ and $G_{\rm IIIC}$ are the critical fracture energies of mode I, II and III, respectively.

Considering the influence of friction on the interface mechanical response, the actual traction τ on the interface is composed of traction τ_s and friction τ_t , as described in [24].

$$\tau = \tau_s + \tau_f \tag{12}$$

Herein, τ_s and τ_f can be determined by Eq. (4.9) and Eq. (4.10), respectively.

$$\tau_s = D_{sr} \delta_r \qquad (s, r = 1, 2, 3)$$
 (13)

$$D_{sr} = \begin{cases} \overline{\delta}_{sr} K & (\delta_{m}^{max} \leq \delta_{m}^{0}) \\ \overline{\delta}_{sr} (1-d) K & (\delta_{m}^{0} < \delta_{m}^{max} < \delta_{m}^{f}, \delta_{1} > 0) \\ \overline{\delta}_{sr} \left[(1-d) K + K d \overline{\delta}_{s1} \right] & (\delta_{m}^{0} < \delta_{m}^{max} < \delta_{m}^{f}, \delta_{1} \leq 0) \\ 0 & (\delta_{m}^{max} \geq \delta_{m}^{f}, \delta_{1} > 0) \\ \overline{\delta}_{s1} \overline{\delta}_{lr} K & (\delta_{m}^{max} \geq \delta_{m}^{f}, \delta_{1} \leq 0) \end{cases}$$

$$(14)$$

where $\, \overline{\!\delta_{ij}} \,$ is the Kronecker operator

$$\begin{cases}
\tau_{f1} = 0 \\
0 & (\delta_{1} \ge 0) \\
0 & (\delta_{m}^{\max} \le \delta_{m}^{0}, \delta_{1} < 0) \\
-\mu K d \delta_{1} \delta_{r} / |\delta_{r}| & (\delta_{m}^{0} < \delta_{m}^{\max} < \delta_{m}^{f}, \delta_{1} < 0) \\
-\mu K \delta_{1} \delta_{r} / |\delta_{r}| & (\delta_{m}^{\max} \ge \delta_{m}^{f}, \delta_{1} < 0)
\end{cases}$$

$$(r = 2, 3)$$

$$(r = 2, 3)$$

Here μ is the interface friction coefficient.

3. Simulation Model

3.1 Architectural parameters and boundary interactions

The finite element software package ABAQUS/Explicit (version 2020) is utilized to construct the finite element model and to examine the damage characteristics of cross-ply sisal composite laminates subjected to low-velocity impact conditions. The finite element model is developed based on the experimental data outlined in reference [25]. The sisal fibre/epoxy composite laminates, measured by a diameter of 75 mm and a thickness of 2 mm, are composed of eight layers, each measuring 0.25 mm, arranged in a stacking sequence of [0/90]2s. To accurately assess the damage characteristics, distinct layers are formulated to represent the cross-ply sisal composite within the laminates. The eight-node solid elements (C3D8R) with reduced integration are employed to discretize each layer. Hourglass control mechanisms have been implemented to mitigate artificial deformation of the elements. For computational accuracy and efficiency, a finer mesh with an element size of 1 mm × 1 mm is employed within the impact zone, while a coarser mesh is utilized in regions outside the impact area. For the simulation of delamination in composite laminates under low-velocity impact, zero-thickness eight-node cohesive elements (COH3D8) are interposed between adjacent layers. Failed cohesive elements are permitted to remain in the model to prevent penetration between the delaminated sections. The cohesive elements and solid elements are interconnected by aggregating the corresponding nodes to ensure the continuity of displacement.

The hemispherical-headed cylindrical impactor, with a diameter of 15 mm, is modeled as an analytical rigid body, allowing for minimal deformation during impact. The impactor is characterized by an initial velocity of 3.5 m/s directed along the z-axis and a concentrated mass of 1.5 kg positioned at its centre, resulting in three unique impact energies of 7.35, 11.03, and 14.70 J. Fixed boundary conditions are imposed along the periphery of the composite laminates, with all degrees of freedom constrained to zero, thus replicating the experimental clamped conditions. Figure 1 shows the finite element model of the sisal cross-ply composite laminates under low-velocity impact. The composite laminates model comprises 38,416 nodes, 18,720 C3D8R elements, and 16,380 COH3D8 elements.

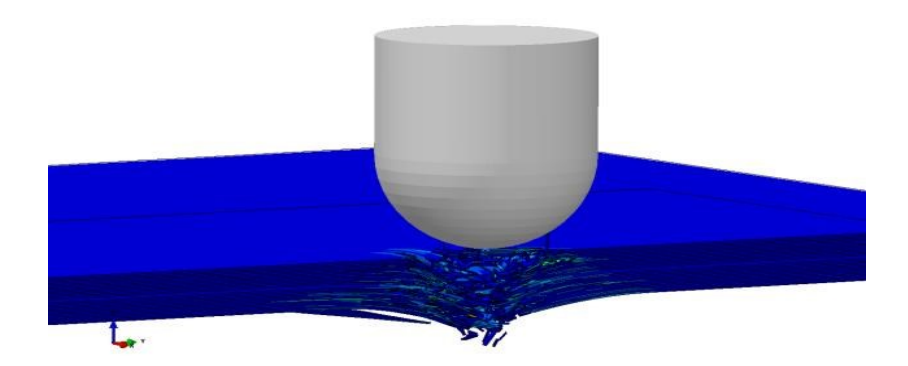


Figure 1. Simulation model of cross-ply sisal/epoxy composite laminates

3.2 Surface interaction and material properties

In the finite element modeling process, 'Surface to Surface Contact', as provided in ABAQUS/Explicit, is employed to delineate the contact response between the impactor and the composite laminates. The penalty contact method, utilizing a finite sliding formulation, is selected to compute the contact force throughout the impact process. The negligible friction between the surfaces of the impactor and the laminates is disregarded. A local coordinate system is established and assigned to each layer. The material properties of the unidirectional composite and the interface cohesive elements utilized in the simulation are referenced [26, 27] and summarized in Tables 1 and 2.

Table 1. Material properties of sisal/epoxy composite laminate				
Density (kg/m ³)	1380			
Laminate properties	$E_{11} = 13.42 \text{ GPa}$; $E_{22} = E_{33} = 5.31 \text{ GPa}$; $v_{12} = v_{13} = 0.32$; $v_{23} = 0.41$			
	$G_{12} = G_{13} = 2.15 \text{ GPa}; G_{23} = 1.73 \text{ GPa}$			
Strength properties (MPa)	X_T =223.15; X_C = 143.21; Y_T = 85.21; Y_C = 61.15;			
Stiffness properties (GPa)	$S_{12} = S_{13} = 13.42$; $S_{23} = 11.92$			
Fracture energy (N/mm)	$G_{fc} = G_{fc} = 10; G_{mc} = G_{mc} = 1$			

Table 2. Material properties of interface cohesive elements

<i>K</i> (N/mm ³)	N (MPa)	S=T (MPa)	$G_{\rm IC}$ (N/mm)	$G_{\text{IIC}} = G_{\text{IIIC}}$ (N/mm)	Density (kg/m³)
2×10 ⁵	62.3	92.3	0.28	0.79	1200

4 Results and Discussion

The composite laminates are subjected to impacts at three distinct energy levels (7 - 15 J). The numerical findings are juxtaposed with the experimental data in Ref. [26] to substantiate the validity of the proposed model. Throughout the impact event, the impact force-time, force-displacement, and energy-time history curves are meticulously recorded, and the intra-laminar matrix cracking and delamination at the interfaces are depicted. Furthermore, the influence of compressive stress-induced interface friction on the initiation and propagation of delamination is thoroughly investigated.

4.1 Validation of numerical model

Figure 2 elucidates the impact force-displacement curves corresponding to three varying impact energy levels. A comparable trend between the numerical simulations and experimental data is discerned across the three energy levels. The maximum displacement predicted by the numerical model consistently exceeds the experimental results by a slight margin. In comparison to the experimental tests, the numerical model exhibits a prolonged duration for contact release, allowing the composite laminates to revert to their initial state more comprehensively. As depicted in Fig. 2 (a-c), it is similarly noted that the maximum displacement of the impactor increases in conjunction with the escalation of impact energy. Notably, the impactor attains its peak displacement value when the impact velocity approaches zero, rather than concurrently with the peak impact force. The displacement of the impactor significantly surpasses the laminates' thickness, attributable to the bending deformation inherent in composite laminates.

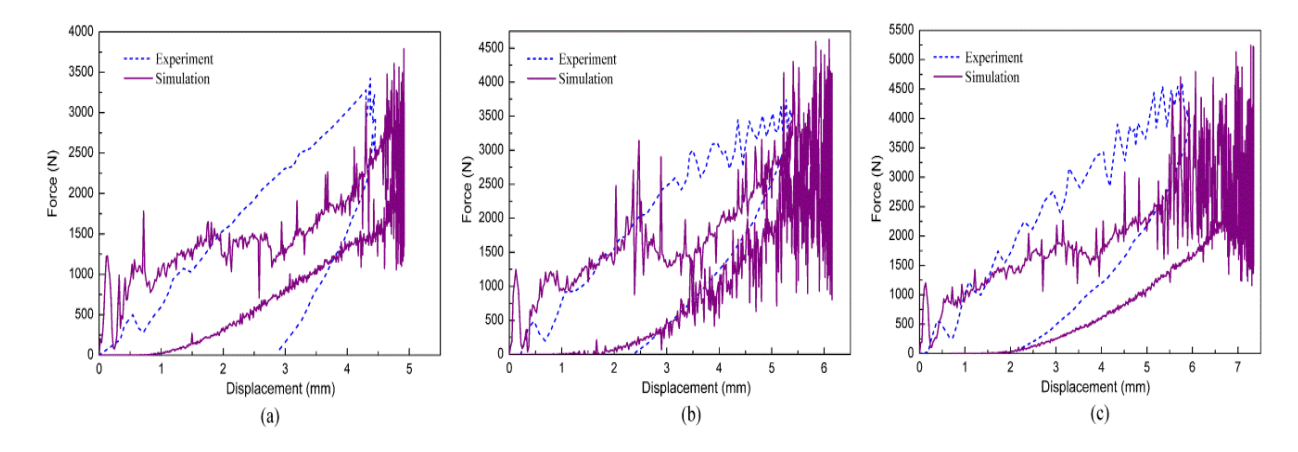


Figure 2. Experimental and numerical impact force-displacement curves compare under different impact energy levels (a) 7.35 J (b) 11.03 J (c) 14.70 J

4.2 Structural impact behaviour

4.2.1 Transient dynamic response

Figure 3 shows that the force experiences an initial sharp increase due to the rapid deceleration of the impactor upon contact with the laminate. This initial increase corresponds to the elastic response exhibited by the material. The tests numerical and experimental reveal a similar trend characterized by a sharp peak followed by a gradual reduction. The maximum force in the simulation result is approximately 6.15 kN, indicative of the material's stiffness and the composite laminate configuration's resistance to deformation, whereas the experimental peak force is observed to be around 5.35 kN, which is marginally lower than the numerical prediction. This discrepancy (~0.8 %) is likely attributable to imperfections present in the experimental samples, such as fibre misalignments, voids, or manufacturing defects, which are not incorporated into the idealized numerical model. Following the peak, the force gradually decreases as damage initiates and propagates within the laminate. Damage mechanisms, including matrix cracking, fibre breakage, and delamination dissipate energy and lower the laminate's load-bearing capacity. The decline is somewhat steeper in the experimental results, potentially due to premature delamination or micro-cracks present in the actual specimens. The close alignment between the numerical and experimental curves validates the precision of the numerical model in forecasting impact behavior. The minor differences observed are within acceptable limits for composite materials subjected to dynamic loading conditions.

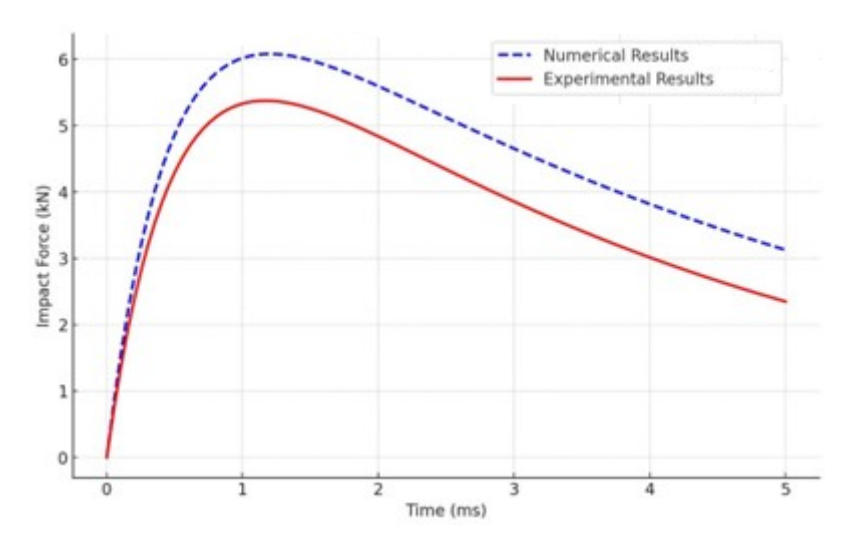


Figure 3. Impact force against time for cross-ply sisal fibre/epoxy composite laminates at 7.35 J

4.2.2 Absorbed energy analysis

The energy-time absorption curve (Figure 4) demonstrates a consistent augmentation as the laminate assimilates the kinetic energy imparted by the impactor through elastic deformation and progressive damage mechanisms. The curve ultimately reaches a plateau, signifying that the majority of the impact energy has been effectively dissipated. From the simulation results, the composite laminate absorbs approximately 95.5 J of energy, which corresponds to approximately 96% of the entire impact energy. Conversely, the empirical test curve indicates an absorbed energy of approximately 96.8 J, marginally exceeding the numerical forecast due to supplementary energy absorption in areas exhibiting minor structural variances. This deviation of approximately 1.3% may be ascribed to supplementary mechanisms, including friction or energy dissipation that were not incorporated in the simulation. This finding is congruent with the pronounced energy-dissipating capacity of sisal fibre/epoxy composites.

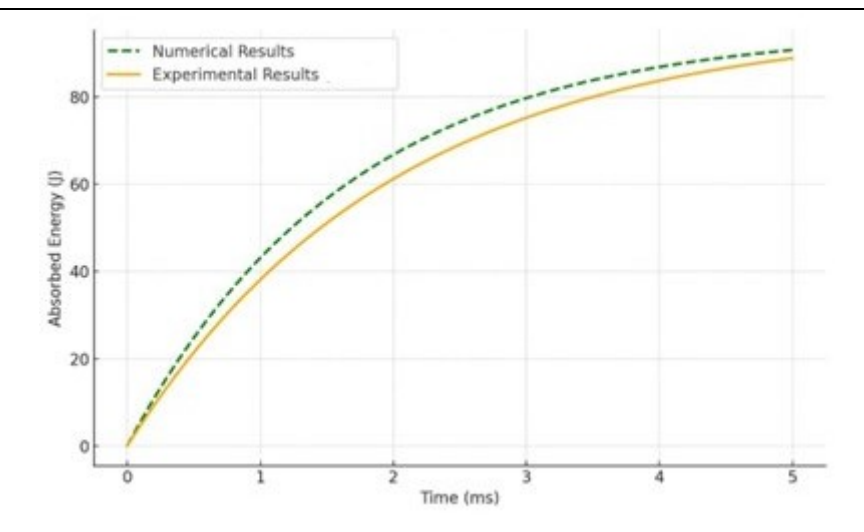


Figure 4. Absorption energy with time for cross-ply sisal fibre/epoxy composite laminates at 7.35 J

4.3 Failure Mechanisms

4.3.1 Stress trajectory

Figure 5 shows the stress distribution within a composite laminate subjected to an impact energy of 14.7 J, illustrated at four distinct time intervals: 2 μ s, 4 μ s, 6 μ s, and 8 μ s. The analysis reveals that at the initial stage (2 μ s), stress is highly concentrated around the impact zone, with moderate stress levels (~6.73 × 10⁸ Pa) localized in proximity to the impact (Figure 5(a)). The laminate commences the process of energy absorption, instigating the propagation of stress waves, as corroborated by [28]. Furthermore, at 4 μ s, the stress levels exhibit a significant increase (~8.43 × 10⁸ Pa), with a broader distribution of stress becoming evident. The regions of peak stress (indicated by red zones) expand radially, reflecting enhanced energy transfer and material response as in Figure 5(b). This phenomenon is in accordance with the observations made by [29, 30], who elucidated the concepts of stress concentration and propagation in impacted composite materials. Also, as indicated in Figure 5(c) at 6 μ s, stress attains its apex magnitude (~9.71 × 10⁸ Pa) near the impact site, coinciding with further outward propagation of stress waves. Structural distortion is apparent, indicating material deformation in response to the applied energy, consistent with investigations into energy dissipation during high-energy impacts [31, 32]. Similarly, Fig. 5(d) at 8 μ s reveals manifestations of stress redistribution, wherein localized regions sustain elevated stress levels while adjacent areas display reduced values (~9.39 × 10⁸ Pa). This phase signifies the material's capacity to manage residual stresses while withstanding considerable deformation as collaborated in Ref. [33].

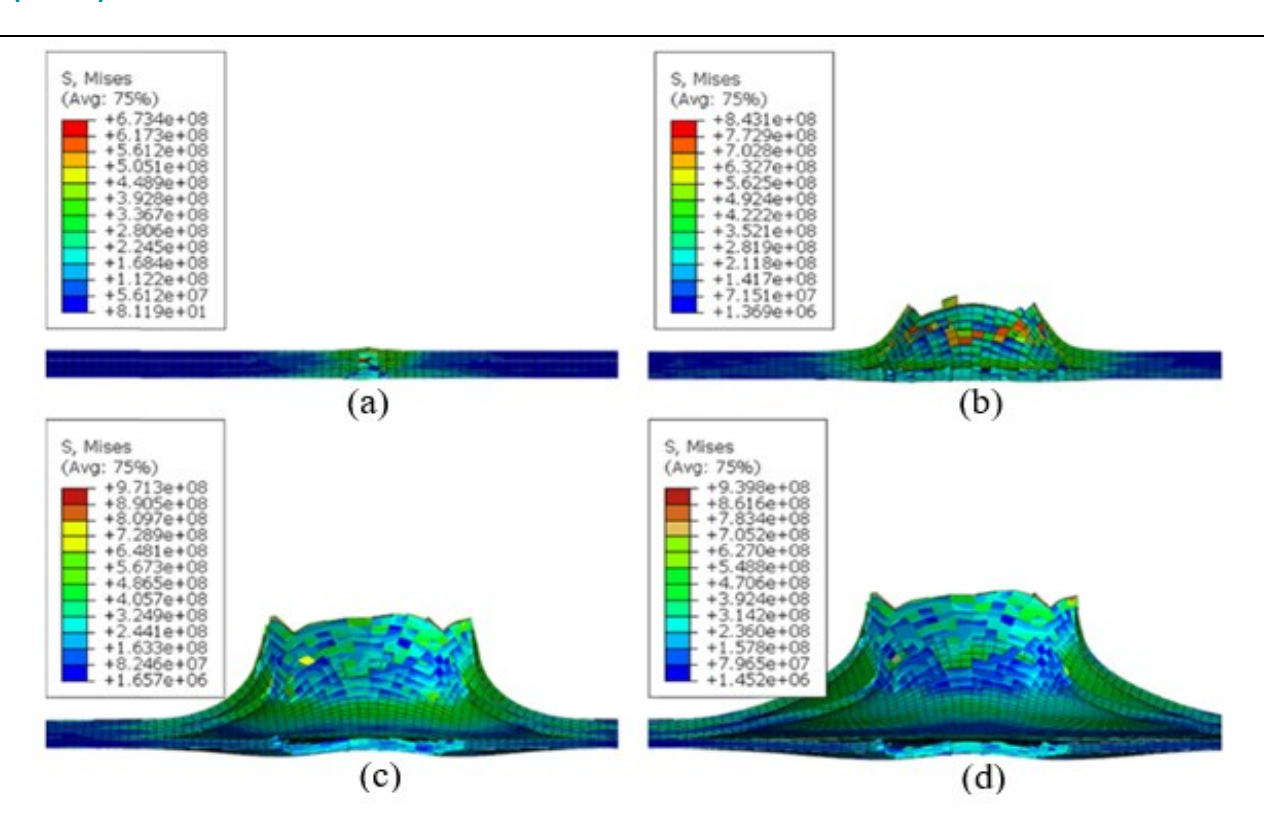


Figure 5. Stress conditions for composite laminate under impact test of 7.35 J (a) 2 µs (b) 4 µs (c) 6 µs (d) 8 µs

4.3.2 Strain condition

The schematic representation provided in Figure 6 elucidates the strain distribution within a composite laminate when subjected to an impact energy of 14.7 J across four temporal intervals: 2 µs, 4 µs, 6 µs, and 8 µs. As seen in Figure 6(a), plastic deformation is predominantly localized within the impact zone, exhibiting low strain levels (approximately 6.56×10^{-3}). This phenomenon signifies the commencement of material yielding, as documented by [34, 35] in their investigations pertaining to composite damage thresholds. Furthermore, it is observable in Figure 6(b) that plastic strain escalates (approximately 1.05×10^{-2}), accompanied by a conspicuous expansion of regions characterized by high strain. The recorded strain values imply the occurrence of localized plastic deformation, which may signify the preliminary stages of damage. Such findings corroborate previous observations regarding delamination and matrix cracking resultant from impact events [36]. It is noteworthy to emphasize in Figure 6(c) that the maximum strain values (approximately 1.29×10^{-2}) are recorded, indicating substantial plastic deformation concentrated around the impact zone. This phase also signifies the progressive accumulation of damage, potentially inclusive of fibre-matrix debonding, as delineated by [37]. Again, in Figure 6(d), the strain zones exhibit stabilization; however, they remain concentrated in proximity to the impact site (approximately 1.23×10^{-2}). This region of heightened plastic strain suggests the potential initiation of failure mechanisms, including delamination and matrix cracking, which are recognized as prevalent failure modes under conditions of high-energy impacts [38].

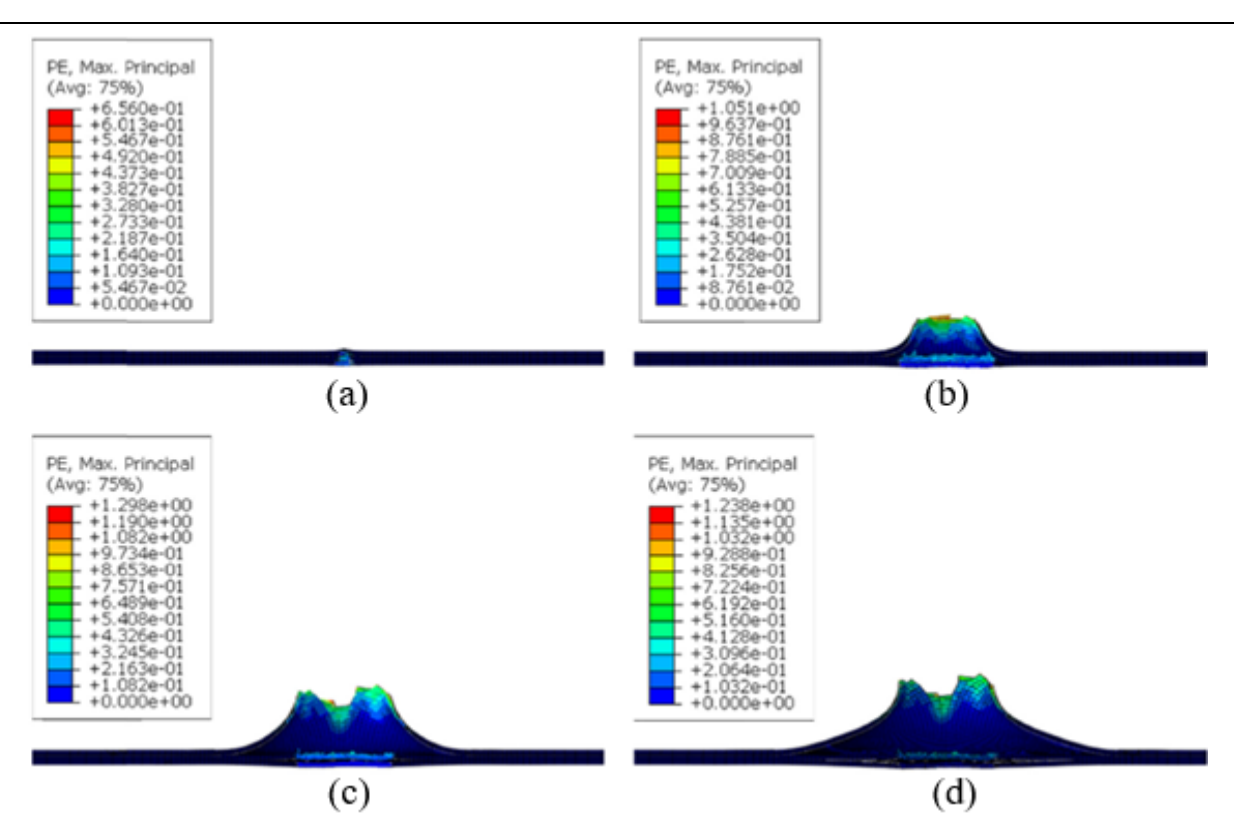


Figure 6. Strain portfolios for composite laminate under impact test of 7.35 J (a) 2 μs (b) 4 μs (c) 6 μs (d) 8 μs

4.3.3 Displacement response

The graphical representations depicted in Figure 7 present displacement contours for a composite laminate subjected to an impact energy of 7.35 J at four temporal intervals (2 μ s - 8 μ s). Figure 7(a) illustrates minimal displacement (approximately 1.18×10^{-3} m), which is localized around the impact zone, reflecting the elastic response exhibited by the material. This observation aligns with the initial phase of elastic deformation as articulated in a study by [39]. In Figure 7(b), there is a notable increase in displacement (approximately 1.69×10^{-2} m), resulting in the formation of a dome-like deformation in the vicinity of the impact site. This deformation indicates a transition towards a plastic response, which is consistent with the findings reported by [40]. Similarly, Figure 7(c) delineates the occurrence of maximum displacement (approximately 1.62×10^{-2} m), with extensive deformation manifesting around the impact location. This phase epitomizes the peak structural response elicited by the applied energy, as corroborated by [41]. Likewise, displacement stabilizes (approximately 1.81×10^{-2} m), with significant deformation evident in the impacted region, as depicted in Figure 7(d). This displacement gradient reflects the mechanisms of energy dissipation, while the residual deformation signifies material failure, as noted in investigations concerning the post-impact behavior of composite materials [42].

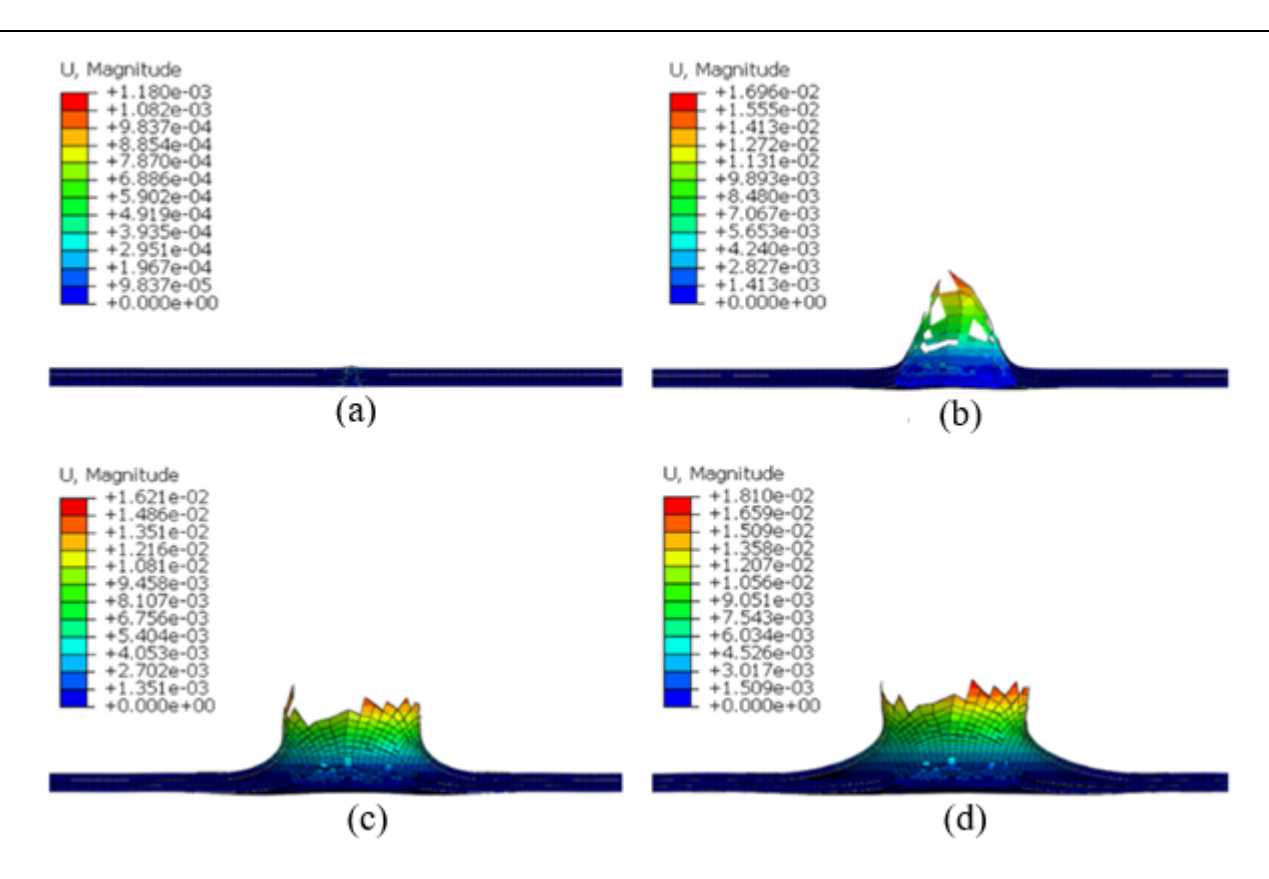


Figure 7. Displacement evolution for composite laminate under impact test of 7.35 J (a) 2 μ s (b) 4 μ s (c) 6 μ s (d) 8 μ s

4.4 Failure Progression

Through the application of finite element modeling, the duration of contact, the extent of deformation, and the propagation of damage is elucidated in detail throughout the entire impact sequence. Figure 8 illustrates the lowvelocity impact behavior of cross-ply composite laminates subjected to an impact energy of 7.35 J. The duration of the impact contact is merely 5 ms; during this impact sequence, various failure modes manifest, interact, and become coupled with one another. From the perspective of damage evolution, the complete impact sequence can be categorized into three distinct phases. (i) The initial phase, characterized as the no-damage period, signifies that no damage occurs within the laminates during this interval, as depicted in Figure 8(a). The impact force experiences a sudden increase from zero as soon as contact is established, resulting in the generation of a compression stress wave that propagates rapidly in both the in-plane and thickness directions of the laminates. Nevertheless, this phase is particularly brief due to the relatively high impact velocity employed in this simulation. (ii) The subsequent phase is the damage propagation period. During this stage, various modes of damage initiate and propagate swiftly within the composite laminates, as illustrated in Figures 8(b-d). The initial manifestation of matrix cracking occurs in the rear layers of the laminates, while matrix crushing is observed in the anterior layers. Delamination is first detected at the upper interfaces and subsequently emerges at all cohesive interfaces. As the impact continues, both matrix cracking and delamination expand persistently; however, no fibre breakage is detected in the layers throughout the entirety of the impact process under this energy level. Due to the ongoing initiation and propagation of damage, the impact force exhibits significant oscillation, and the rate of increase of the impact force begins to decelerate. This phase concludes when the impact velocity of the impactor reaches zero. (iii) The final phase is termed the impact rebound period. In this phase, the impact force progressively diminishes, and the impactor consistently rebounds, as represented in Figures 8(e-f). The bending deformation induced in the laminates by the impact recovers gradually.

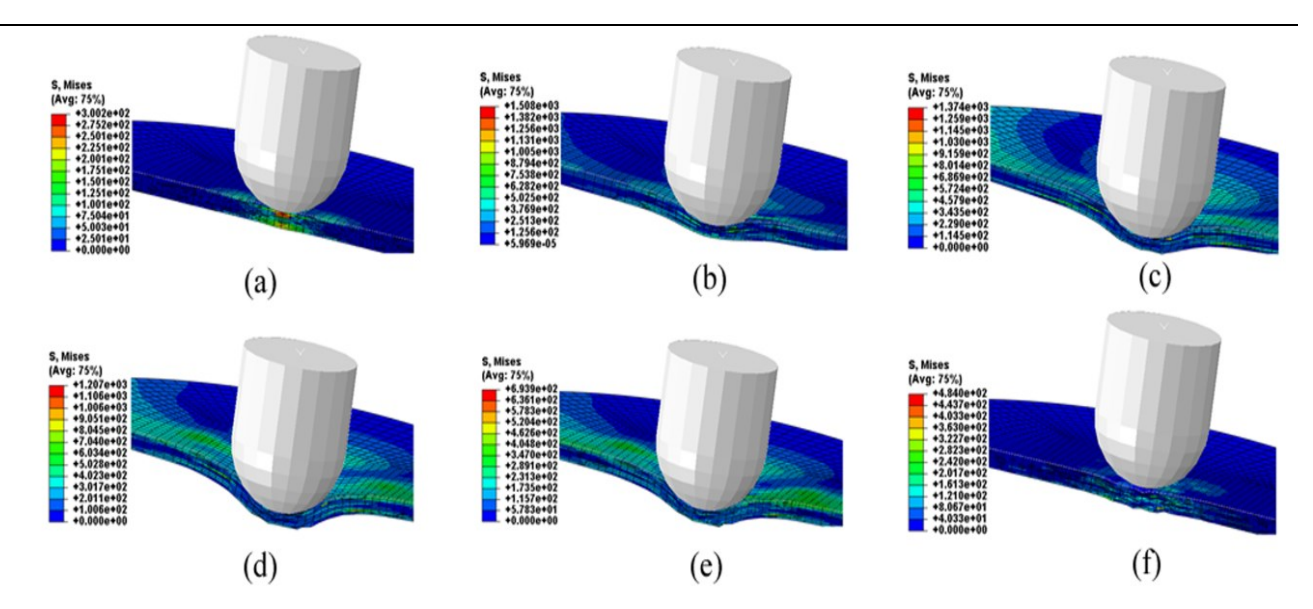


Figure 8. Damage progression for sisal/epoxy composite laminates under impact energy of 7.35 J (a) 0.05 ms (b) 0.7 ms (c) 1.4 ms (d) 2.1 ms (e) 3.5 ms (f) 5.0 ms

In summary, under this energy level, the matrix cracking within the layers ceases to propagate, whereas the laminates continue to develop new interface delamination to a certain extent for a limited duration.

5. Conclusion

This investigation offers a thorough numerical analysis of cross-ply sisal fibre/epoxy composite laminates subjected to low-velocity impact loading. By integrating cohesive elements within the finite element modelling framework, the study provides significant insights into the delamination and energy absorption characteristics of these bio-composites. The results underscore the potential of sisal/epoxy laminates as sustainable alternatives for structural applications, while simultaneously accentuating the necessity for further optimization of cohesive parameters and laminate configurations. Future research endeavours could investigate the incorporation of hybrid fibres and the ramifications of varying strain rates to enhance material performance.

Acknowledgments

The author would like to acknowledge all the authors for their manuscript contributions.

References

- [1] S. Kumar, L. Prasad, V.K. Patel, V. Kumar, A. Kumar, A. Yadav, J. Winczek, Physical and mechanical properties of natural leaf fiber-reinforced epoxy polyester composites, Polymers 13(9) (2021) 1369.
- [2] A.R. Bhat, R. Kumar, P.K.S. Mural, Natural fiber reinforced polymer composites: a comprehensive review of tribo-mechanical properties, Tribology International (2023) 108978.
- [3] R.V. Patel, A. Yadav, J. Winczek, Physical, mechanical, and thermal properties of natural fiber-reinforced epoxy composites for construction and automotive applications, Applied Sciences 13(8) (2023) 5126.
- [4] A. Ekhtiyari, M.M. Shokrieh, A novel rate-dependent cohesive zone model for simulation of mode I dynamic delamination in laminated composites, Composite Structures 281 (2022) 114962.
- [5] M. Linke, R. Lammering, On the calibration of the cohesive strength for cohesive zone models in finite element analyses, Theoretical and Applied Fracture Mechanics 124 (2023) 103733.
- [6] D. Quan, G. Zhao, G. Scarselli, R. Alderliesten, Co-curing bonding of carbon fibre/epoxy composite joints with excellent structure integrity using carbon fibre/PEEK tapes, Composites Science and Technology 227 (2022) 109567.
- [7] N. Xu, C. Lu, T. Zheng, S. Qiu, Y. Liu, D. Zhang, D. Xiao, G. Liu, Enhanced mechanical properties of carbon fibre/epoxy composites via in situ coating-carbonisation of micron-sized sucrose particles on the fibre surface, Materials & Design 200 (2021) 109458.

- [8] D. Mamalis, C. Floreani, C.M.Ó. Brádaigh, Influence of hygrothermal ageing on the mechanical properties of unidirectional carbon fibre reinforced powder epoxy composites, Composites Part B: Engineering 225 (2021) 109281.
- [9] D. Quan, U. Farooq, G. Zhao, C. Dransfeld, R. Alderliesten, Co-cured carbon fibre/epoxy composite joints by advanced thermoplastic films with excellent structural integrity and thermal resistance, International Journal of Adhesion and Adhesives 118 (2022) 103247.
- [10] E.A. Duodu, Simulation of Quasi-Isotropic E-Glass Composite Laminate at Low Velocity Impact with Cohesive Interface Elements, Journal of Science & Technology (JST) 5(6) (2020) 128-140.
- [11] A. Ammar, W. Leclerc, M. Guessasma, N. Haddar, Discrete element approach to simulate debonding process in 3D short glass fibre composite materials: Application to PA6/GF30, Composite Structures 270 (2021) 114035.
- [12] D. kumar Gara, G. Raghavendra, P.S. Prasad, S. Ojha, Enhanced mechanical properties of glass fibre epoxy composites by 2D exfoliated graphene oxide filler, Ceramics International 47(24) (2021) 34860-34868.
- [13] A.S. Al-Azzawi, C. Featherston, C. Lupton, C. Jiang, A. Barouni, U. Koklu, K. Giasin, Impact characteristics of S2-glass fibre/FM94-epoxy composites under high and cryogenic temperatures: Experimental and numerical investigation, Composites Part B: Engineering 287 (2024) 111786.
- [14] E. Achimnole, E. Orhorhoro, M. Onogbotsere, Simulation of Gas Turbine Power Plant Using High Pressure Fogging Air Intake Cooling System, International Journal of Emerging Engineering Research and Technology 5(5) (2017) 16-23.
- [15] I. Shah, J. Li, S. Yang, Y. Zhang, A. Anwar, Experimental investigation on the mechanical properties of natural fiber reinforced concrete, Journal of Renewable Materials 10(5) (2022) 1307.
- [16] U.L. Ezeamaku, O.D. Onukwuli, M.E. Ezeh, I.O. Eze, N.E. Odimegwu, C.P. Agu, Experimental investigation on influence of selected chemical treatment on banana fibre, Industrial Crops and Products 185 (2022) 115135.
- [17] M.S. Siddiqui, M. Rabbi, S. Dewanjee, Low-velocity impact response of natural fibre reinforced composites: a comprehensive review on influential parameters, Composites Part C: Open Access (2023) 100422.
- [18] M.H. Mulla, M.N. Norizan, C.K. Abdullah, N.F.M. Rawi, M.H.M. Kassim, N. Abdullah, M.N.F. Norrrahim, M.S.M. Elahi, Low velocity impact performance of natural fibre reinforced polymer composites: a review, Functional Composites and Structures 5(3) (2023) 035004.
- [19] M.S. Shaik, H.S. Subramanian, An experimental investigation on low-velocity impact response of abaca/epoxy bio-composite, Journal of Natural Fibers 19(13) (2022) 6977-6992.
- [20] M.R. Karim, Constitutive modeling and failure criteria of carbon-fiber reinforced polymers under high strain rates, The University of Akron, 2005.
- [21] S. Murakami, Mechanical modeling of material damage, ASME, Transactions, Journal of Applied Mechanics 55 (1988) 280-286.
- [22] I. Lapczyk, J.A. Hurtado, Progressive damage modeling in fiber-reinforced materials, Composites Part A: Applied Science and Manufacturing 38(11) (2007) 2333-2341.
- [23] F. Guo-dong, L. Jun, W. Bao-lai, Progressive damage and nonlinear analysis of 3D four-directional braided composites under unidirectional tension, Composite Structures 89(1) (2009) 126-133.
- [24] G. Alfano, E. Sacco, Combining interface damage and friction in a cohesive-zone model, International Journal for Numerical Methods in Engineering 68(5) (2006) 542-582.
- [25] Y. Shi, T. Swait, C. Soutis, Modelling damage evolution in composite laminates subjected to low velocity impact, Composite structures 94(9) (2012) 2902-2913.
- [26] K. Senthilkumar, N. Saba, N. Rajini, M. Chandrasekar, M. Jawaid, S. Siengchin, O.Y. Alotman, Mechanical properties evaluation of sisal fibre reinforced polymer composites: A review, Construction and Building Materials 174 (2018) 713-729.
- [27] S. Long, X. Yao, X. Zhang, Delamination prediction in composite laminates under low-velocity impact, Composite Structures 132 (2015) 290-298.
- [28] S. Syed Abdullah, Low velocity impact testing on laminated composites, Impact studies of composite materials, Springer2021, pp. 1-17.
- [29] S. Abrate, B. Castanié, Y.D. Rajapakse, Dynamic failure of composite and sandwich structures, Springer Science & Business Media2012.
- [30] S. Abrate, J.-F. Ferrero, P. Navarro, Cohesive zone models and impact damage predictions for composite structures, Meccanica 50 (2015) 2587-2620.

- [31] Y. Zhang, Z. Zhu, R. Joseph, I.J. Shihan, Damage to aircraft composite structures caused by directed energy system: A literature review, Defence Technology 17(4) (2021) 1269-1288.
- [32] V. Allheily, F. Lacroix, A. Eichhorn, L. Merlat, G. L'Hostis, B. Durand, An experimental method to assess the thermo-mechanical damage of CFRP subjected to a highly energetic 1.07 µm-wavelength laser irradiation, Composites Part B: Engineering 92 (2016) 326-331.
- [33] K. Liew, Z. Pan, L. Zhang, An overview of layerwise theories for composite laminates and structures: Development, numerical implementation and application, Composite Structures 216 (2019) 240-259.
- [34] D. Lai, C. Demartino, Y. Xiao, High-strain rate compressive behavior of fiber-reinforced rubberized concrete, Construction and Building Materials 319 (2022) 125739.
- [35] A. Ahmed, M.Z. Rahman, Y. Ou, S. Liu, B. Mobasher, S. Guo, D. Zhu, A review on the tensile behavior of fiber-reinforced polymer composites under varying strain rates and temperatures, Construction and Building Materials 294 (2021) 123565.
- [36] P. FERABOLI, K.T. KEDWARD, A multi-parameter approach to impact performance characterization, Dynamic Effects in Composites 1 (2012) 1.
- [37] R.A. Shanks, Modelling of polymeric fibre-composites and finite element simulation of mechanical properties, Finite Element Analysis (2010) 285-314.
- [38] S. Shah, S. Karuppanan, P. Megat-Yusoff, Z. Sajid, Impact resistance and damage tolerance of fiber reinforced composites: A review, Composite Structures 217 (2019) 100-121.
- [39] C. Sun, M.N. Saleh, An introduction to the impact damage of composite materials, Non-destructive Testing of Impact Damage in Fiber-Reinforced Polymer Composites, Elsevier2024, pp. 1-41.
- [40] Y. Huang, F.T. EShun, J. Hu, X. Zhang, J. Zhao, S. Zhang, R. Qian, Z. Chen, D. Chen, Research on low-velocity impact response of novel short-fiber-reinforced composite laminates, Polymers 15(4) (2023) 840.
- [41] B. Liu, F. Li, Y. Liu, Y. Zhang, Experimental and numerical studies on low-velocity impact of laminated C/SiC structures, Composite Structures 329 (2024) 117765.
- [42] U. Khashaba, A comprehensive analysis of low velocity impact response of [0/±45/90] s thin woven GFRP composites at room temperature, Composite Structures 339 (2024) 118160.